JOURNAL OF PROPULSION AND POWER
Vol. 27, No. 4, July–August 2011

Thrust Stand Characterization of the NASA Evolutionary Xenon Thruster

Kevin D. Diamant,* James E. Pollard,† and Mark W. Crofton‡
The Aerospace Corporation, El Segundo, California 90245
and
Michael J. Patterson§ and George C. Soulas¶
NASA John H. Glenn Research Center at Lewis Field, Cleveland, Ohio 44135

DOI: 10.2514/1.B34095

Direct thrust measurements have been made on the NASA Evolutionary Xenon Thruster using a standard pendulum-style thrust stand constructed specifically for this application. Values have been obtained for the full 40-level throttle table, as well as for a few offnominal operating conditions. Measurements differ from the nominal NASA throttle table 10 values by 3.1% at most, while at 30 throttle levels, the difference is less than 2.0%. When measurements are compared with throttle table 10 values that have been corrected using recently obtained ion beam current density and charge-state data, they differ by 1.2% at most, and at 37 throttle levels, they differ by 1.0% or less. Thrust correction factors calculated from direct thrust measurements and from recently acquired plume data agree to within measurement error for all but one throttle level. Measurements of thrust due to cold flow, neutralizer, and discharge-only operation are also presented.

Nomenclature

A_e	=	neutralizer exit aperture area
$\bar{c}$	=	neutral mean thermal speed
C_{cf}	=	cold flow thrust correction for offaxis flow
D	=	dimension
d	=	dimension
D_C	=	dimension
D_S	=	dimension
F_C	=	calibration force
F_{cf}	=	cold flow thrust
F_n	=	neutralizer thrust
F_S	=	load cell reading
F_T, F	=	thrust
g	=	acceleration due to gravity at sea level
H	=	dimension
J_b	=	ion beam current
k	=	Boltzmann constant, also ratio of specific heats
l	=	distance from pivot to counterweight center of mass
L_C	=	dimension
L_{CG}	=	distance from pivot to thruster center of mass
L_F	=	distance from pivot to thruster centerline
L_S	=	dimension
M_e	=	moments due to gas and electrical connections
m_{CW}	=	counterweight mass
$\dot{m}_d$	=	discharge chamber mass flow rate
m_n, m	=	neutral atomic mass
$\dot{m}_n$	=	neutralizer mass flow rate
m_T	=	thruster mass
p_e	=	pressure at neutralizer exit
q	=	elementary charge
R	=	accelerator grid aperture radius, also specific gas constant
t	=	accelerator grid aperture thickness
T_n	=	neutral gas temperature
T_o	=	neutralizer gas stagnation temperature
u_e	=	neutralizer gas effective exhaust velocity
V_b	=	ion beam voltage
V_{bps}	=	beam power supply voltage
X_C	=	dimension
X_S	=	dimension
Y	=	dimension
α	=	angle
β	=	thrust correction factor for beam divergence
γ	=	total thrust correction factor
δ	=	dimension
ε	=	angle relative to aperture centerline
θ	=	pendulum angle
ϕ	=	angle
ψ	=	angle from grid centerline

Presented as Paper 2010-6701 at the 46th AIAA/ASME/SAE/ASEE Joint Propulsion Conference and Exhibit, Nashville, TN, 25–28 July 2010; received 25 August 2010; revision received 28 January 2011; accepted for publication 31 January 2011.

*Research Scientist, Propulsion Science, M2-341. Senior Member AIAA.
†Senior Scientist, Propulsion Science, M2-341.
‡Senior Scientist, Propulsion Science, M2-341. Senior Member AIAA.
§Senior Technologist for In-Space Propulsion, Mail Stop 16-1. Member AIAA.
¶Electrical Engineer, Propulsion and Propellants Branch, Mail Stop 16-1.

I. Introduction

NASA's Evolutionary Xenon Thruster (NEXT) is engineered to be extremely flexible in terms of input power and specific impulse while maintaining acceptable efficiency, and it embodies a number of advances over previous ion engine systems. Some of its operating characteristics are being examined in detail through a program described in [1], of which this work is a part.

The NEXT throttle table was developed for missions outside of Earth orbit, and it incorporates 40 levels to account for varying solar power with sun–spacecraft separation. Before this work, thrust has been estimated from terminal parameters and available plume data. Recent plume measurements [2] have improved the fidelity of those estimates; however, direct thrust measurements are needed for benchmarking.

The majority of thrust measurements reported in the electric propulsion literature have been made indirectly by measuring deflection of the mechanism to which the thruster is mounted and converting that deflection to thrust through some suitable calibration. The mechanism is generally a pendulum, either standard [3–7], inverted [8–10], or torsional [11–14], and calibration is accomplished

through application of a set of weights. By contrast, high-thrust chemical engines are generally tested with load cells (e.g., [15]). The availability of load cells with sufficient sensitivity permitted their introduction by Crofton [16] to low-thrust measurement applications. Advantages conferred through the use of load cells are high accuracy over a wide measurement range due to their high degree of linearity, the limiting of thrust stand motion to very small values, and prompt readings. With regard to the latter, there is no need for time-consuming force-displacement calibrations, during which thermal drift may introduce uncertainty into the measurement. The use of load cells for low-thrust measurements has been demonstrated in [17–19], and it is the method adopted here to measure thrust due to ion beam extraction. However, the sensitivity required to accurately measure thrust during operation without ion beam extraction (cold flow, neutralizer, and discharge-only) exceeded the capability of the load cell, and those measurements were made using an inclinometer along with a set of calibration weights.

II. Test Apparatus

Measurements were performed in a 2.4-m-diam × 9.8-m-long cryopumped vacuum chamber with the thruster oriented along the chamber centerline. Two reentrant pumps were on the end-dome behind the thruster, two more reentrant pumps were in the beam dump region, and four 1.3 m cryotubs were mounted on the cylindrical wall of the tank adjacent to the thruster. The base pressure with no gas load was less than 1×10^{-5} Pa, with 90% of the residual gas being water vapor and the remainder being air and hydrocarbons. The beam dump was lined with carbon composite sheets and flexible graphite to minimize the yield of sputtered material. Lab power supplies and a lab propellant feed system were used to operate the PM1R prototype model thruster. Background pressure was measured by an ionization gauge located on the tank wall adjacent to the thruster. With an 1800-V 3.52-A beam, the xenon pressure was 4.8×10^{-4} Pa, applying the correction factor of 0.348 specified by the gauge manufacturer for xenon relative to nitrogen. The effective pumping speed for this condition was 2.1×10^5 liter/s, well in excess of the roughly 1.4×10^5 liter/s needed to ensure that the rate of ingestion of background gas was less than 1% of the propellant supply flow.

Figure 1 shows the main features of the thrust stand, consisting of a standard pendulum with a hardened steel knife edge pivot, a counterweight, a high-precision inclinometer, and an eddy current damper. Electrical power was carried by highly flexible, finely stranded, polyvinyl chloride insulated 22 American wire gauge wires. Multiple wires were used so that the maximum current per wire was 1.75 A. The eddy current damper consisted of an aluminum plate suspended below the thruster on an aluminum rod. The plate swung through the gap between the 5.1-cm-high × 10.2-cm-wide poles of a permanent magnet assembly consisting of two pairs of NdFeB magnets. The damping force was enhanced by arranging the pairs to produce a field reversal at the center of the assembly (Fig. 2). By experimentation, it was found that a 0.64-mm-thick aluminum plate provided nearly critical damping at a gap such that the maximum magnetic field magnitude at the center of the gap was 0.33 T. Perhaps, due to the action of the damper, there was no detectable effect of facility vibration on the output of the inclinometer or load cell.

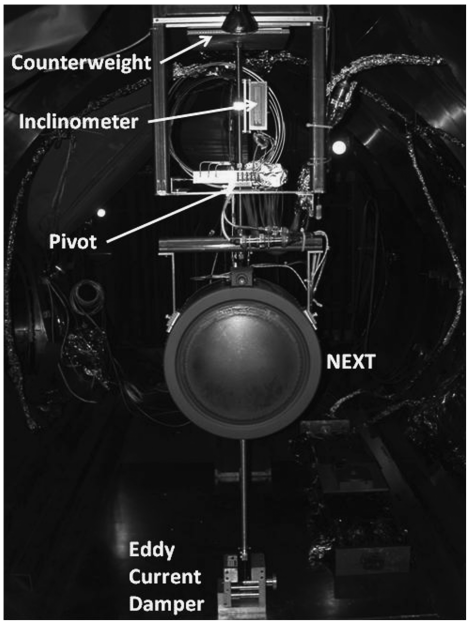

Fig. 1 Thrust stand.

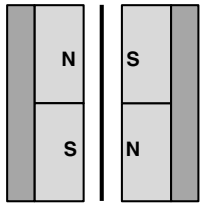

Fig. 2 Top view of damper showing magnets (light shading) arranged to produce a field reversal at the center of the assembly. Heavy black line represents the aluminum plate.

The load cell was mounted to a translation stage and connected to the back of the thruster, at thruster centerline, by a length of 50-lb-test braided fishing line (Fig. 3). Thrust was measured by translating the load cell until the tension in the line exceeded the anticipated thrust. This was done while running the neutralizer and main discharge but without ion beam extraction (discharge-only mode). The difference in line tension created by energizing the grids yielded a measurement of thrust due to ion beam extraction. Multiple measurements were obtained in a relatively short time by cycling the grid voltages. This strategy sought to minimize thermal drift of the thrust stand by obtaining prompt readings (typically, the switching transient died out within 10–15 s, and a steady reading was recorded for 1–2 min) and by minimizing the change in currents and power to the thruster.

The load cell sensitivity was not adequate to accurately measure thrust in discharge-only mode or with cold flow alone. However, by adjustment of the counterweights, it was possible to obtain those measurements using the inclinometer.

III. Analysis and Calibration

The diagram shown in Fig. 4 was used to determine the relations needed to reduce the raw data for thrust due to ion beam extraction. The pendulum is shown inclined by an angle θ (positive sense as shown) from the vertical. The mass distributed above the pivot m_{CW} is assumed to be concentrated at some location that we will call the counterweight center of mass, and that below the pivot m_T is assumed to be concentrated at a location we will call the thruster center of mass. The braided line connected the load cell (marked "s" for sensor) to a stud protruding from the back of the thruster on the thruster centerline. The monofilament connected the thruster to a

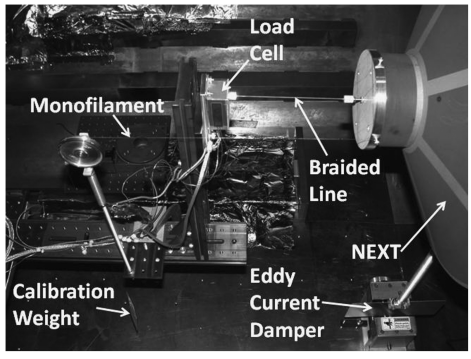

Fig. 3 Thrust stand operation with load cell.

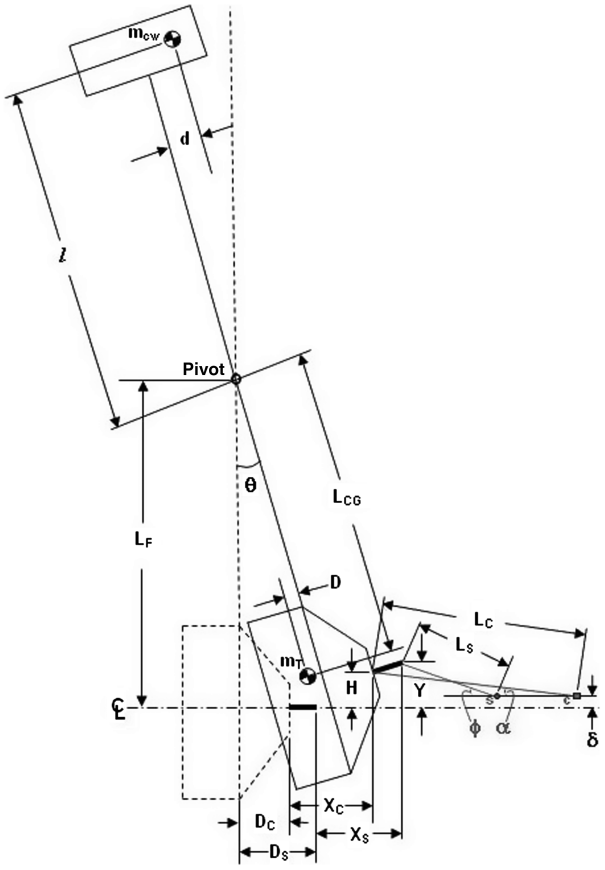

Fig. 4 Measurement schematic.

calibration weight strung over a pulley. The location of the top of the pulley is marked "c" (for calibration), and the point of attachment to the thruster is at the height of the thruster centerline but offset in the horizontal plane (Fig. 3). The thrust stand was insensitive to such an offset.

For thrust measurements, the monofilament was absent, and summing moments about the pivot (at steady state, $\dot{\theta} = \ddot{\theta} = 0$) yields

$$F_T L_F + F_S(L_F - Y)\cos\phi - F_S(X_S + D_S)\sin\phi - m_T g(L_{CG}\sin\theta - D\cos\theta) + m_{CW} g(l\sin\theta - d\cos\theta) + \Sigma M_e = 0 \quad (1)$$

where F_T is thrust, assumed to act normal to the grid surface at thruster centerline, F_S is the tension in the braided line, $\sum M_e$ represents moments due to the gas and electrical connections, and g is the acceleration due to gravity at sea level. The counterweight was set so that the magnitudes of θ and ϕ were, at most, 0.5 and 1.5°, respectively, and the small angle approximations ($\cos\phi = \cos\theta = 1$, $\sin\phi = \phi$, and $\sin\theta = \theta$) are valid. If we further neglect terms that are second order in θ and neglect $\delta L_F\theta$ relative to δD_S (δ is the vertical offset between the load cell and thruster centerline), Eq. (1) becomes

$$F_T + F_S\left[1 + \frac{\delta D_S}{L_S L_F} - \frac{D_S}{L_F}\theta\left(1 + \frac{D_S}{L_S}\right)\right] - \frac{1}{L_F}[m_T g(L_{CG}\theta - D) - m_{CW} g(l\theta - d) - \Sigma M_e] = 0 \quad (2)$$

where δ is nominally zero and will be important only in the uncertainty analysis.

F_T was determined by writing Eq. (2) once with ion beam extraction, once without, and subtracting. This procedure would have been relatively more simple if the inclination θ was constant, with and without ion beam extraction. In practice, it was found to vary by a very small amount (0.002 to 0.013°), but it was large enough to require inclusion in the analysis. This variation, corresponding to linear displacements from approximately 0.02 to 0.13 mm, arose roughly in equal parts from stretch in the braided line and in the strain-gauge-based load cell. In any case, subtraction of Eq. (2) with beam extraction from Eq. (2) without beam extraction yields

$$F_T = \Delta F_S\left[1 + \frac{\delta D_S}{L_S L_F} - \frac{D_S}{L_F}\theta_{avg}\left(1 + \frac{D_S}{L_S}\right)\right] - g\left(m_T\frac{L_{CG}}{L_F} - m_{CW}\frac{l}{L_F}\right)\Delta\theta \quad (3)$$

where Δ indicates a difference in two readings, θ_{avg} is the average inclination, and $\sum M_e$ is assumed constant over the very small variation in θ. To arrive at this form, it was necessary to assume the following:

$$\frac{D_S}{2}(F_{S1} + F_{S2})\left(1 + \frac{D_S}{L_S}\right) \ll g(m_T L_{CG} - m_{CW} l) \quad (4)$$

where F_{S1} and F_{S2} are readings with and without beam extraction, respectively. The validity of this assumption will be demonstrated shortly.

Equation (3) shows that, in addition to load cell and inclinometer calibrations, knowledge of the mass properties of the pendulum was needed to calculate thrust. The arrangement shown in Fig. 2 was used at ambient conditions to calibrate the mass properties. Simulating a thrust measurement, the load cell was translated to produce tensions in the braided line slightly in excess of the desired simulated thrusts, and then weights were hung from the monofilament line, relieving tension in the braided line. With reference to Fig. 3, summing moments about the pivot at steady state yields

$$F_C(L_F - H)\cos\alpha - F_C(D_C + X_C)\sin\alpha + F_S(L_F - Y)\cos\phi - F_S(X_S + D_S)\sin\phi - m_T g(L_{CG}\sin\theta - D\cos\theta) + m_{CW} g(l\sin\theta - d\cos\theta) + \Sigma M_e = 0 \quad (5)$$

where F_C is the tension in the monofilament line. After applying the small angle approximations (magnitude of α was less than 0.5°), neglecting terms that are second order in θ and neglecting $\delta L_F\theta$ relative to δD_S and δD_C, Eq. (5) becomes

$$F_C\left[1 + \frac{\delta D_C}{L_C L_F} - \frac{D_C}{L_F}\theta\left(1 + \frac{D_C}{L_C}\right)\right] + F_S\left[1 + \frac{\delta D_S}{L_S L_F} - \frac{D_S}{L_F}\theta\left(1 + \frac{D_S}{L_S}\right)\right] - \frac{1}{L_F}[m_T g(L_{CG}\theta - D) - m_{CW} g(l\theta - d) - \Sigma M_e] = 0 \quad (6)$$

As before, we write Eq. (6) twice and subtract, yielding

$$g\left(m_T\frac{L_{CG}}{L_F} - m_{CW}\frac{l}{L_F}\right) = \frac{1}{\Delta\theta}\left\{\Delta F_C\left[1 + \frac{\delta D_C}{L_C L_F} - \frac{D_C}{L_F}\theta_{avg}\left(1 + \frac{D_C}{L_C}\right)\right] + \Delta F_S\left[1 + \frac{\delta D_S}{L_S L_F} - \frac{D_S}{L_F}\theta_{avg}\left(1 + \frac{D_S}{L_S}\right)\right]\right\} \quad (7)$$

To arrive at this form, it was necessary to assume

$$\frac{D_C}{2}(F_{C1} + F_{C2})\left(1 + \frac{D_C}{L_C}\right) \approx \frac{D_S}{2}(F_{S1} + F_{S2})\left(1 + \frac{D_S}{L_S}\right) \ll g(m_T L_{CG} - m_{CW} l) \quad (8)$$

The right-hand side (RHS) of Eq. (7) involves the difference (ΔF_C and ΔF_S are of opposite signs) of two nearly equal numbers, resulting in large uncertainty in the calculated mass properties. Therefore, 84 measurements were averaged, yielding a value of 8.6×10^3 mN for the left-hand side (LHS) of Eq. (7), and thereby a value of 4.8×10^5 mN · cm for the RHS of Eq. (8) ($L_F = 56.4$ cm). The LHS of Eq. (8) has a maximum value of 3.8×10^3, validating Eqs. (4) and (8).

The inclinometer was calibrated under vacuum, with the thruster operating, by displacing the thruster known amounts using a rod attached to a linear translation stage. The load cell was calibrated at ambient conditions with a series of seven weights ranging from 2.5 to 24.5 g (24.6 to 241 mN) and spanning the nominal throttle table thrust range (25.6 to 236.4 mN). The load cell and inclinometer were heated and controlled to their ambient operating temperatures (25.5 ± 0.2 and 21.0 ± 0.2°C for the load cell and inclinometer, respectively) while under vacuum.

Calibration for cold flow and discharge-only thrust measurements was performed under vacuum with the familiar arrangement in which a series of weights was lowered by a motor over a pulley and the response of the stand (in this case a change in inclination) was recorded. Ten 51 mg washers were used as calibration weights.

IV. Results

A. Discharge-Only Cold Flow

We will attempt to model the thrust produced by the neutral gas flowing from the discharge chamber of an ion thruster under the condition of zero input power using an expression of the form

$$F_{\mathrm{cf}} = C_{\mathrm{cf}} \dot{m}_d \bar{c} \tag{9}$$

where F_{cf} is the cold flow thrust, C_{cf} is a factor that accounts for offaxis flow, $\dot{m}_d$ is the discharge chamber mass flow rate, and $\bar{c}$ is the mean thermal speed of the neutrals given by

$$\bar{c} = \sqrt{\frac{8kT_n}{\pi m_n}} \tag{10}$$

where k is the Boltzmann constant, T_n is the neutral gas temperature, and m_n is the gas molecular mass.

Ion thruster discharge chambers operate within the free molecular flow regime. For the case of flow through thin-walled apertures, the cosine law of molecular effusion applies [20]. In the case of a flat grid, we obtain

$$C_{\mathrm{cf}} = \frac{\int_0^{\pi/2} \cos^2(\varepsilon)\sin(\varepsilon)\,\mathrm{d}\varepsilon}{\int_0^{\pi/2} \cos(\varepsilon)\sin(\varepsilon)\,\mathrm{d}\varepsilon} \tag{11}$$

where ε is the angle relative to aperture centerline. This expression integrates to the simple result $C_{\mathrm{cf}} = \frac{2}{3}$.

A more realistic analysis must account for finite aperture thickness, grid curvature, and the presence of two grids. The two cylindrical apertures that a neutral particle must pass through to escape the discharge chamber present a difficult problem to model. Fortunately, Kuharski et al. modeled a two-cylindrical-aperture set that had a geometry that was very similar to that of the NEXT thruster [21]. They found that the angular distribution of particles exiting the accelerator grid was well modeled by assuming a single accelerator grid cylindrical aperture. This simplification was possible because of the large screen aperture diameter and low thickness relative to that of the accelerator grid. This same simplifying assumption will be employed here.

Clausing was the first to develop an expression for the angular distribution of particles downstream of a cylindrical aperture [22]. His equation assumes that the aperture is a point source and that the flux of particles from the walls of the aperture is linear as a function of axial thickness, which is a very accurate assumption over a range of aperture thickness-to-radius ratios that span from zero to about eight [23]. The angular distribution of particles downstream of a cylindrical aperture $T_c(\varepsilon)$ in the far field is given by [22,24]

$$T_c(\varepsilon) = \begin{cases} 1 - \left\{ \dfrac{2}{\pi}(1-\kappa)\left[\arcsin\left(\dfrac{t\tan(\varepsilon)}{2R}\right) + \dfrac{t\tan(\varepsilon)}{2R}\sqrt{1-\left(\dfrac{t\tan(\varepsilon)}{2R}\right)^2} \right] \right\} + \dfrac{4}{3\pi}(1-2\kappa)\dfrac{1-[1-\{[t\tan(\varepsilon)]/2R\}^2]^{3/2}}{[t\tan(\varepsilon)]/2R} & \text{if } \varepsilon \le \arctan\left(\dfrac{2R}{t}\right) \\ \kappa + \dfrac{4}{3\pi}\dfrac{1-2\kappa}{\frac{t\tan(\varepsilon)}{2R}} & \text{if } \varepsilon > \arctan\left(\dfrac{2R}{t}\right) \end{cases} \tag{12}$$

where

$$\kappa = \frac{\sqrt{t^2+4R^2} - t}{2R + [4R^2/\sqrt{t^2+4R^2}]} \tag{13}$$

Here, t is the accelerator aperture thickness, ε is the angle that the velocity makes with the aperture centerline, and R is the accelerator grid aperture radius. The contribution to C_{cf} from a single aperture is obtained from

$$C_{\mathrm{cf,hole}} = \frac{\int_0^{\pi/2} T_c(\varepsilon)\cos^2(\varepsilon)\sin(\varepsilon)\,\mathrm{d}\varepsilon}{\int_0^{\pi/2} T_c(\varepsilon)\cos(\varepsilon)\sin(\varepsilon)\,\mathrm{d}\varepsilon} \tag{14}$$

The total C_{cf} can be found by correcting the contribution per hole for offaxis thrusting due to grid curvature:

$$C_{\mathrm{cf}} = C_{\mathrm{cf,hole}} \frac{\int_0^{\psi_{\max}} \cos(\psi)\sin(\psi)\,\mathrm{d}\psi}{\int_0^{\psi_{\max}} \sin(\psi)\,\mathrm{d}\psi} \tag{15}$$

where ψ is the angle from grid centerline and $\psi_{\max}$ is the angle to the edge of the accelerator grid perforated pattern. This analysis assumes that the upstream neutral density is uniform over the grid. For a NEXT accelerator grid, the correction factor C_{cf} is found to be 0.720.

Measured values of cold flow discharge-only thrust (no flow to the neutralizer) are shown in Fig. 5. These measurements were obtained by cycling the flow on and off and noting the change in thrust stand inclination. Six readings were taken and averaged at each flow rate. The selected flow rates correspond to throttle levels (TLs) 12, 27, and 40. Measurements were taken after the thruster sat under steady vacuum conditions overnight and before the application of any electrical power. The thrust stand frame temperature was −11°C, and this was taken to be the temperature of the thruster and of the neutral gas. By including the point (0, 0) and fitting the data to a straight line, we obtain $C_{\mathrm{cf}} = 0.74$, in excellent agreement with the theoretically derived value.

B. Neutralizer Only

Neutralizer thrust was measured (again by cycling on and off) for the case of warm neutral flow (heater at the ignition current level but no plasma) and for a 3 A keeper discharge. The measurements include a correction factor of 2.0 to account for the difference between the neutralizer-to-pivot moment arm and that between the point of application of the calibration weights (thruster centerline) and the pivot. We will attempt to model both cases using a continuum fluid approach (neutralizer internal pressure $\sim\mathcal{O}(10^3)$ Pa), and we will initially consider a purely thermal thrust mechanism, for which thrust can be estimated from

$$F_n = \dot{m}_n u_e + p_e A_e \tag{16}$$

where F_n is the neutralizer thrust, $\dot{m}_n$ is the neutralizer flow rate, u_e is the effective exhaust velocity, p_e is the pressure at the neutralizer exit aperture, and A_e is the exit aperture area (ambient pressure is assumed to be negligible). If we assume an isentropic expansion to a Mach number of one at the exit plane, we obtain

$$F_n = \dot{m}_n \sqrt{kRT_o} \left(\frac{2}{k+1}\right)^{1/2} \left(1 + \frac{1}{k}\right) \tag{17}$$

where k is the ratio of specific heats, R is the specific gas constant, and T_o is the gas stagnation temperature.

For the warm flow case, at a xenon flow rate of 10 standard cubic centimeters per minute (sccm) and assumed stagnation temperature of 1100°C [Eq. (17)] yields a predicted thrust of 0.52 mN. The measured value at 10 sccm (average of five measurements) was also 0.52 mN, with an estimated uncertainty of 16%. Ten sccm is a larger than nominal neutralizer flow and was selected to improve the measurement signal-to-noise ratio without any expectation of altering the physics.

For the case of a 3 A keeper discharge (heater turned off), the flow rate was 6 sccm, and the measured thrust (average of six measurements) was 0.41 mN with an estimated uncertainty of 18%. At $F_n = 0.41$ mN and $\dot{m}_n = 6$ sccm, Eq. (17) yields a prediction of 2360 K for T_o. Neutral temperatures near this value have been experimentally observed [25] and predicted by numerical simulation [26,27] in the region near the exit aperture of a hollow cathode. Alternatively, it has been suggested that electron pressure (i.e., ambipolar ion acceleration) may contribute significantly to hollow cathode thrust [28]. Using measured values of plasma density (10^{21} m^{-3}) and electron temperature (2 eV) from the NASA Solar Electric Propulsion Technology Application Readiness (NSTAR) hollow cathode [29], we estimate that this contribution could be approximately 0.1 mN. Summing this value with the result from Eq. (17) under the assumption that the neutrals remain at a wall temperature of 1100°C yields a total thrust of approximately 0.4 mN. We should note that a contribution of 0.1 mN is very close to the estimated absolute uncertainty (0.07 mN) in our measurement.

C. Discharge-Only with Plasma

Thrust was measured with power supplied to the main discharge chamber but with the screen and accelerator grid power supplies turned off. The neutralizer ran continuously at 6 sccm with a 3 A keeper discharge during this experiment, while the main discharge (power and flow) was cycled on and off to determine its contribution to thrust. Main discharge run times were kept short (less than 1 min) to minimize heating of the thrust stand in an attempt to avoid thermal drifting. Nevertheless, thermal drifting was observed to be significant on the time scale of the measurements, probably as a result of changes in electrical cable tension. The contribution to the change in thrust stand inclination due to the cables was estimated in the following way. Following shutdown of the main discharge power and flow, the rate of change of thrust stand inclination with time was determined at a point at which the gas flow had diminished to 5–10% of its steady value, as determined by vacuum chamber pressure readings (thrust assumed to be negligible at that point). This rate was assumed to apply during the period of thrust cessation, and it was multiplied by the time required to get to 5–10% of steady flow to obtain the contribution from the cables. This was then subtracted from the total inclination change over that same period to obtain the main discharge contribution. In our error analysis, we arbitrarily assigned an uncertainty of 50% to the inclination change due to the cables.

Results are shown in Fig. 6 for a range of discharge-only power levels spanning those found in the nominal throttle table. Each point represents the average of two to five measurements. It is evident that thrust scales linearly with discharge power and that values are significantly greater than those found with cold flow (Fig. 5). If we assume that thrust is generated by the escape of thermal neutrals and apply the analysis from Sec. IV.A (with $C_{cf} = 0.74$), we find that neutral temperatures from 2100 to 5600 K are required. This finding conflicts with the common assumption that the neutral gas accommodates to the thruster wall temperature [30] that, for NEXT, does not exceed approximately 530 K in the steady state [31].

Measurements of the accelerator grid potential during discharge-only operation show that it is within a few volts of the cathode potential, indicating that discharge ions may escape and produce thrust as they accelerate through the plasma-to-ground potential

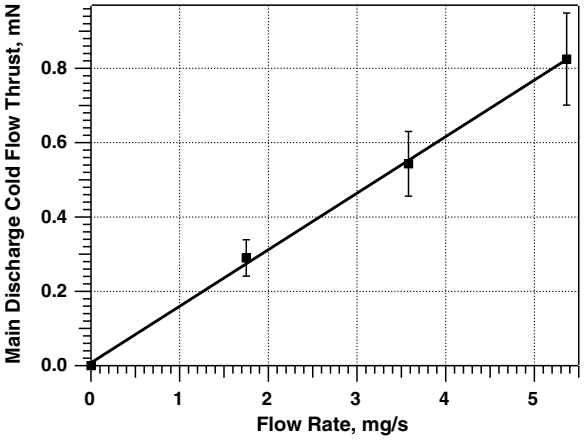

Fig. 5 Discharge-only cold flow thrust; temperature = −11°C.

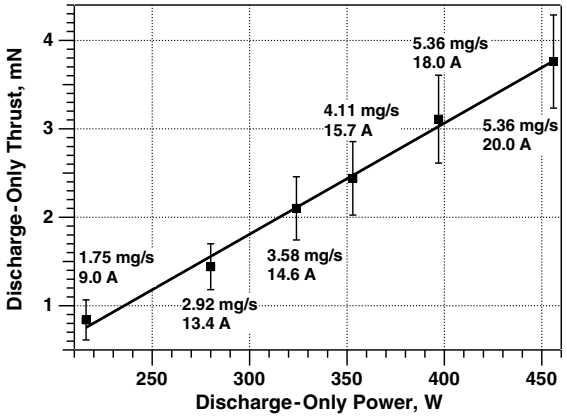

Fig. 6 Discharge-only thrust (discharge mass flow and current listed next to each data point).

difference. Based on plasma densities and electron temperatures recorded near the grids during discharge-only operation [32], thrust of several micronewtons appears possible; however, an accurate estimate requires an analysis of ion trajectories through the grids (i.e., determination of an effective grid system transparency) and is beyond the scope of this work.

Other nonthermal mechanisms appear to be less plausible. High energy neutrals can be produced by charge exchange with ions accelerating through the sheath upstream of the screen grid but with Debye lengths on the order of 0.01 to 0.1 mm [33], sheath thickness on the order of 10 Debye lengths [34], and estimated charge exchange mean free paths on the order of 10 cm for a 25 eV ion; this

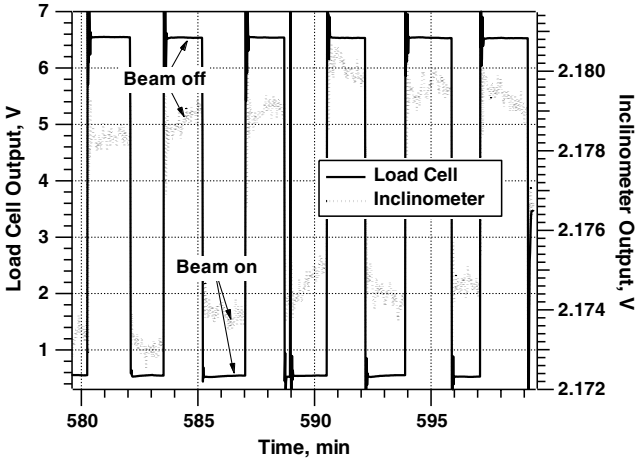

Fig. 7 Sample ion beam thrust measurement raw data; TL 32.

Table 1 Values for uncertainty analysis

Parameter	Typical value	Absolute uncertainty	Percentage uncertainty
L_F, cm	56.4	0.25	
L_C, cm	38.9	0.25	
L_S, cm	14.6	0.25	
D_C, cm	24.4	0.25	
D_S, cm	28.2	0.25	
ϑ_{avg}, °	−0.4 to 0.8	0.0008	
$\Delta\vartheta$, °	0.002 to 0.015	0.0008	
δ, cm	0	0.13	
ΔF_C , mN	24 to 240	0.001	
ΔF_S , mN	24 to 240		0.14

mechanism is estimated to account for less than 10% of the observed thrust. Ions created in the vicinity of the cathode with energies (relative to the cathode) in excess of the discharge voltage could escape directly or escape as neutrals following charge exchange collisions; however, for cathodes studied in simulated discharge chamber environments, those ions tend not to be axially directed [35–37].

D. Ion Beam

Thrust due to ion beam extraction was measured for the complete 40-level throttle table by the load cell method described in Secs. II and III. Sample raw data (six on–off cycles) from TL 32 are shown in Fig. 7. Six measurements were taken at each TL, with the exception

Table 2 Thrust comparison

TL	V_{bps}, V	$F_{measured}$, mN	F_{TT10}, mN	Corrected F_{TT10}, mN	$F_{measured}$– F_{TT10}, %	$F_{measured}$–Corrected F_{TT10}, %	$\sigma/F_{measured}$, %	$F_{measured}$ uncertainty, %
					$m_d = 1.56$ mg/s, $J_b = 1.00$ A			
1	275	25.4	25.6	25.4	−0.8	−0.3	0.2	1.1
					$m_d = 1.75$ mg/s, $J_b = 1.20$ A			
2	300	31.4	31.9	31.5	−1.6	−0.5	0.6	1.2
3	400	37.1	37.2	37.0	−0.4	0.4	0.5	1.2
4	650	47.9	48.2	47.7	−0.5	0.5	0.2	1.0
5	679	49.1	49.2	48.9	−0.2	0.5	0.3	1.1
6	850	54.5	55.2	54.6	−1.2	−0.2	0.2	0.9
7	936	56.9	57.9	57.1	−1.7	−0.3	0.2	0.9
8	1021	59.2	60.5	59.6	−2.1	−0.6	0.2	0.8
9	1179	63.4	65.1	63.9	−2.5	−0.7	0.2	0.8
10	1396	68.8	70.8	69.5	−2.8	−0.9	0.2	0.8
11	1567	72.9	75.1	73.7	−2.9	−1.1	0.1	0.7
12	1800	77.9	80.3	78.8	−3.1	−1.2	0.1	0.7
					$m_d = 2.33$ mg/s, $J_b = 1.60$ A			
13	1021	79.6	80.6	79.4	−1.3	0.3	0.2	0.8
14	1179	85.1	86.8	85.3	−2.0	−0.2	0.0	0.8
15	1396	92.3	94.5	92.8	−2.3	−0.6	0.1	0.7
16	1567	97.7	100.1	98.4	−2.5	−0.8	0.3	0.6
17	1800	104.4	107.0	105.2	−2.5	−0.8	0.1	0.6
					$m_d = 2.92$ mg/s, $J_b = 2.00$ A			
18	1021	100.3	100.7	99.5	−0.4	0.8	0.2	0.8
19	1179	107.0	108.4	106.7	−1.2	0.3	0.1	0.8
20	1396	115.9	117.9	115.9	−1.7	0.0	0.1	0.7
21	1567	122.6	125.0	122.9	−1.9	−0.3	0.3	0.7
22	1800	130.9	133.9	131.8	−2.3	−0.6	0.1	0.7
					$m_d = 3.58$ mg/s, $J_b = 2.35$ A			
23	1021	118.9	118.9	118.1	0.0	0.7	0.1	0.8
24	1179	127.0	128.0	126.5	−0.8	0.3	0.2	0.7
25	1396	137.4	139.4	137.6	−1.4	−0.1	0.1	0.7
26	1567	145.2	147.5	145.6	−1.6	−0.2	0.1	0.7
27	1800	155.2	157.9	155.8	−1.7	−0.4	0.2	0.7
					$m_d = 4.11$ mg/s, $J_b = 2.70$ A			
28	1021	137.1	136.6	135.8	0.4	1.0	0.2	0.8
29	1179	146.4	146.9	145.4	−0.4	0.7	0.1	0.7
30	1396	158.5	160.0	157.9	−0.9	0.4	0.1	0.7
31	1567	167.1	169.4	167.1	−1.4	0.0	0.1	0.7
32	1800	178.4	181.4	178.9	−1.6	−0.3	0.1	0.7
					$m_d = 4.72$ mg/s, $J_b = 3.10$ A			
33	1179	168.6	168.7	167.2	−0.1	0.9	0.1	0.7
34	1396	182.5	183.7	181.4	−0.6	0.6	0.1	0.7
35	1567	192.6	194.4	191.8	−0.9	0.4	0.1	0.7
36	1800	205.5	208.4	205.5	−1.4	0.0	0.0	0.7
					$m_d = 5.36$ mg/s, $J_b = 3.52$ A			
37	1179	192.4	191.8	190.2	0.3	1.2	0.1	0.7
38	1396	208.0	208.8	206.4	−0.4	0.8	0.2	0.7
39	1567	219.4	220.7	217.9	−0.6	0.7	0.1	0.7
40	1800	234.6	236.9	233.6	−1.0	0.4	0.1	0.7

of TLs 5, 9, 13, and 18, for which 11, 18, 7, and 7 measurements were taken, respectively. The neutralizer ran continuously at 6 sccm with a 3 A keeper discharge during this experiment. The thruster was warmed up daily before data collection by operating at either TL 5 or TL 9 for 3.5 to 4 h, or at TL 37 for 2 to 2.5 h.

Table 1 lists typical values and uncertainties for the parameters involved in data reduction. The quoted uncertainties for the various lengths (except δ) reflect the practical difficulty of making measurements on and around the thruster. The uncertainty in δ is the displacement observed to occur as a result of vacuum-atmosphere cycling on the facility. Noise on the inclinometer output determined the uncertainties in θ_{avg} and $\Delta\theta$, and that in ΔF_C was determined by the accuracy of the scale used to weigh the calibration weights. The results of the load cell calibration ΔF_S show an average uncertainty of 0.14% over the tested range (24.6 to 241 mN). Thrust uncertainty was dominated by terms containing δ, a situation which, in hindsight, could have been most easily avoided by using a longer braided line.

E. Total Thrust

Total thrust was calculated by summing the contributions from ion beam extraction (Sec. IV.D), the main discharge without beam extraction (Sec. IV.C), and the neutralizer without beam extraction (Sec. IV.B). Main discharge-only thrust was determined by applying the linear fit shown in Fig. 6 to measured discharge-only power at each TL.

Table 2 contains the results F_{measured} for the 40 NEXT TLs. These are compared with values calculated using thrust correction factors from the NASA throttle table 10 (TT10) F_{TT10} and using thrust correction factors obtained from plume data reported in [2] (corrected F_{TT10}). F_{measured} represents measurement averages, and σ is the measurement standard deviation. V_{bps} is the beam power supply (screen supply) voltage. Standard methods for propagating uncertainties [38] were employed to arrive at the values shown in the final column of Table 2.

We should note that, in our comparison to the TT10 values, the neutralizer thrust contribution is applied in an approximate manner. The neutralizer flow rate of 6 sccm differs from the nominal TT10 values, which range from 2.5 to 4.0 sccm (6 sccm was chosen to ensure that the keeper discharge would not extinguish during extended periods with no ion beam extraction). Also, the change in neutralizer thrust between operation, with and without ion beam extraction, was only partially captured (due to the smaller neutralizer-pivot moment arm) by the measurements from Sec. IV.D. Fortunately, neutralizer thrust is small, and these inaccuracies are likely to fall within the quoted total thrust measurement uncertainties.

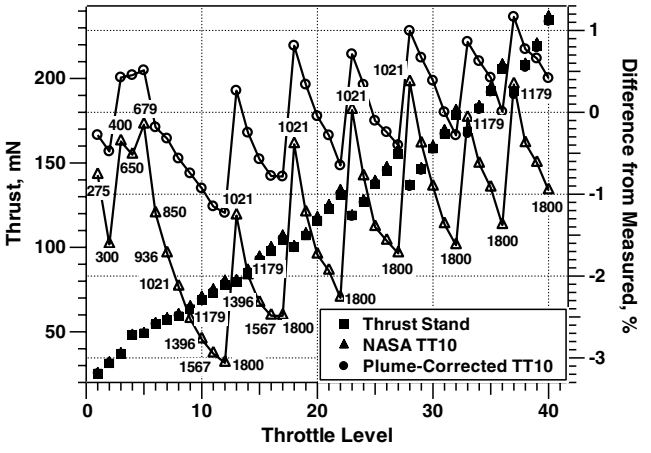

Fig. 8 Measured (thrust stand) and predicted total thrust. Open symbols represent differences between the measured values and the NASA TT10 (triangles) and plume-corrected TT10 (circles) predictions. Measured–NASA TT10 trace annotated with beam power supply voltages.

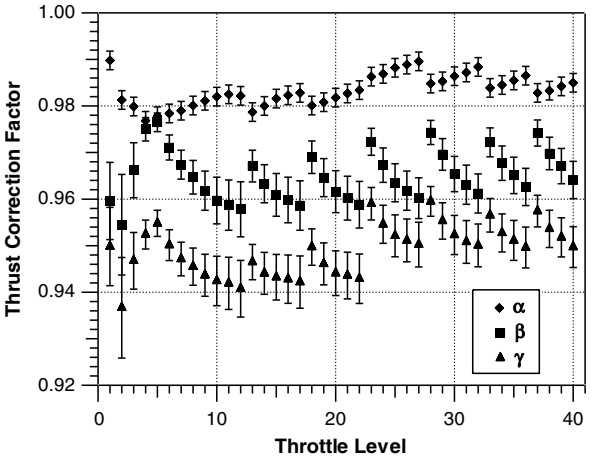

Fig. 9 PM1R thrust correction factors for doubly charged ions α, beam divergence β, and their product γ vs TL (from [2]).

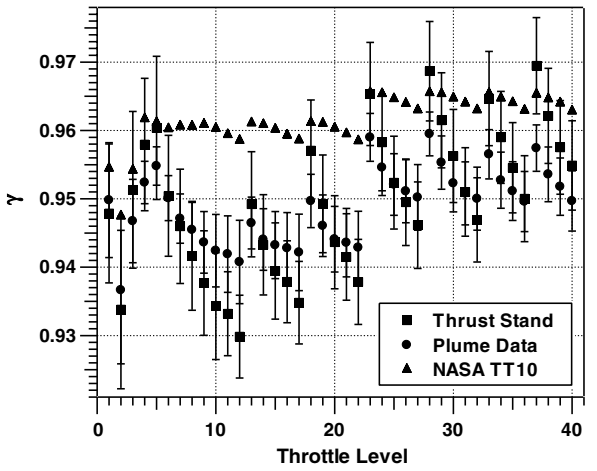

Fig. 10 Thrust correction factors from the nominal NASA TT10, calculated from plume ion flux and charge-state measurements [2], and from direct thrust measurements.

The data from Table 2 are plotted in Fig. 8. The structure in the difference traces is nearly identical in form to that of the thrust correction factor due to beam divergence β calculated from the plume data [2] (Fig. 9). This implies a proportionality between the two, and it suggests the need for additional plume measurements to improve the fidelity of β. Another explanation for the difference trace structure, which seems less probable (because it does not explain

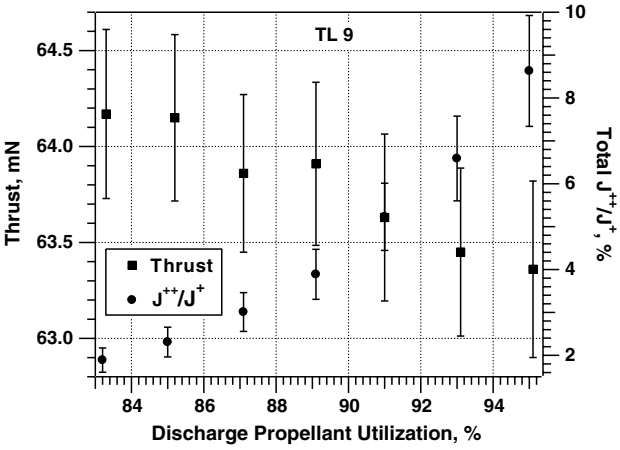

Fig. 11 Thrust and total J^{++}/J^{+} (J^{++}/J^{+} from [2]) vs utilization at TL 9.

TLs 2–5), is that the true ion beam current was reduced due to backstreaming of plume electrons to the anode. Backstreaming, possibly through the perforated ground screen, is favored by increasing beam supply voltage.

Figure 10 compares thrust correction factors γ obtained from thrust stand measurements to those derived from the plume current density [2] and charge-state measurements, and to the NASA TT10 values. The thrust correction factor γ accounts for thrust losses due to beam divergence and multiply charged ions, and it is defined by the well-known expression for the thrust F of an ion engine:

$$F = \gamma J_b \sqrt{2mV_b/q} \tag{18}$$

where J_b is the ion beam current, V_b is the ion beam voltage (equal to V_{bps} less the neutralizer coupling voltage), m is the ion mass, and q is the elementary charge. Plotting γ allows us to observe that the error bars for the thrust-stand-derived values and those calculated from plume data overlap for the entire throttle table with the exception of TL 37. This represents remarkably good agreement for measurements made by independent methods.

Figure 11 shows measured thrust as a function of discharge chamber propellant utilization (ratio of ion beam current to discharge chamber mass flow expressed in equivalent amperes) for TL 9 (nominal discharge propellant utilization for TL 9 is 93%). Taken alone, the increasing doubly ionized current fraction (J^{++}/J^{+}) should result in a 1.8% decrease in thrust over the examined range [2], which compares favorably with the 1.3% decrease in measured thrust (the data required to determine thrust corrections due to beam divergence are not available at these operating conditions).

V. Conclusions

Direct thrust measurements have been made on the NASA NEXT ion engine and compared with the NASA TT10 for the full set of 40 TLs, as well as for a few offnominal operating conditions. Measurements differ from the nominal TT10 values by 3.1% at most, while at 30 TLs, the difference is less than 2.0%. When measurements are compared with the TT10 values corrected with ion beam current density and charge-state data from [2], they differ by 1.2% at most, and at 37 TLs, by 1.0% or less. Thrust correction factors γ calculated from direct thrust measurements and from plume data from [2] agree to within measurement error for all but one of the TLs.

Measurements of cold flow thrust and thrust with plasma present but without ion beam extraction have been made for the main discharge and neutralizer. Analytical expressions are given that allow accurate thrust estimation in the absence of plasma. With plasma present, electrostatic ion acceleration may contribute significantly to thrust for both the main discharge and neutralizer.

Acknowledgments

This work was supported under The Aerospace Corporation's Independent Research and Development Program. The authors thank Kevin McCormick of NASA John H. Glenn Research Center at Lewis Field for outstanding technical support throughout the process of thruster installation and Mike Worshum, Tom Albright, and Dave Rikimaru of The Aerospace Corporation for many excellent suggestions and outstanding technical support in the development and construction of the thrust stand. Robert Csortos of Dura Magnetics, Inc., designed the eddy current damper magnet assembly. Special thanks go to George Valenzuela of The Aerospace Corporation for explaining some of the finer points of fishing line usage and to Dan Herman of the NASA John H. Glenn Research Center at Lewis Field for many helpful suggestions.

References

[1] Crofton, M. W., Pollard, J. E., Beiting, E. J., Spektor, R., Diamant, K. D., Eapen, X. L., Cohen, R. B., and Patterson, M. J., "Characterization of the NASA NEXT Thruster," AIAA Paper 2009-4815, Aug. 2009.

[2] Pollard, J. E., Diamant, K. D., Crofton, M. W., Patterson, M. J., and Soulas, G. C., "Spatially-Resolved Beam Current and Charge-State Distributions for the NEXT Ion Engine," AIAA Paper 2010-6779, July 2010.

[3] Banks, B., Rawlin, V., Weigand, A., and Walker, J., "Direct Thrust Measurement of a 30-cm Ion Thruster," AIAA Paper 1975-340, March 1975.

[4] Komurasaki, K., and Arakawa, Y., "Hall Current Ion Thruster Performance," AIAA Paper 1990-2594, July 1990.

[5] Fisch, N. J., Raitses, Y., Litvak, A. A., and Dorf, L. A., "Design and Operation of Hall Thruster with Segmented Electrodes," AIAA Paper 1999-2572, June 1999.

[6] Beiting, E. J., "Impulse Thrust Stand for MEMS Propulsion Systems," AIAA Paper 1999-2720, June 1999.

[7] Markusic, T. E., Jones, J. E., and Cox, M. D., "Thrust Stand for Electric Propulsion Performance Evaluation," AIAA Paper 2004-3441, July 2004.

[8] Haag, T. W., "Design of a Thrust Stand for High Power Electric Propulsion Devices," AIAA Paper 1989-2829, July 1989.

[9] Haag, T. W., and Curran, F. M., "High Power Hydrogen Arcjet Performance," AIAA Paper 1991-2226, June 1991.

[10] Welle, R. P., Pollard, J. E., Janson, S. W., Crofton, M. W., and Cohen, R. B., "One Kilowatt Hydrogen and Helium Arcjet Performance," AIAA Paper 1991-2229, June 1991.

[11] Choueiri, E. Y., and Ziemer, J. K., "Quasi-Steady Magneto-plasmadynamic Thruster Performance Database," *Journal of Propulsion and Power*, Vol. 17, No. 5, Sept.–Oct. 2001, pp. 967–976. doi:10.2514/2.5857

[12] Ziemer, J. K., "Performance Measurements Using a Sub-Micronewton Resolution Thrust Stand," International Electric Propulsion Conference, Electric Rocket Propulsion Soc. Paper 01-238, Fairview Park, OH, Oct. 2001.

[13] Gamero-Castano, M., and Hruby, V., "Using a Torsional Balance to Characterize Thrust at Micronewton Levels," AIAA Paper 2003-4537, July 2003.

[14] Marhold, K., and Tajmar, M., "Micronewton Thrust Balance for Indium FEEP Thrusters," AIAA Paper 2005-4387, July 2005.

[15] Brimhall, Z. N., Divitotawela, N., Atkinson, J. P., Kirk, D. R., and Peebles, H. G., "Design and Validation of a Six Degree of Freedom Rocket Motor Test Stand," AIAA Paper 2008-5051, July 2008.

[16] Crofton, M. W., "Evaluation of Electric Thrusters," The Aerospace Corp. Rept. ATR-97(8201)-1, El Segundo, CA, April 1997.

[17] Diamant, K. D., Pollard, J. E., Cohen, R. B., Raitses, Y., and Fisch, N. J., "Segmented Electrode Hall Thruster," *Journal of Propulsion and Power*, Vol. 22, No. 6, Nov.–Dec. 2006, pp. 1396–1401. doi:10.2514/1.19417

[18] Diamant, K. D., Zeigler, B. L., and Cohen, R. B., "Microwave Electrothermal Thruster Performance," *Journal of Propulsion and Power*, Vol. 23, No. 1, Jan.–Feb. 2007, pp. 27–34. doi:10.2514/1.19571

[19] Diamant, K. D., Pollard, J. E., Raitses, Y., and Fisch, N. J., "Ionization, Plume Properties, and Performance of Cylindrical Hall Thrusters," *IEEE Transactions on Plasma Science*, Vol. 38, No. 4, April 2010, pp. 1052–1057. doi:10.1109/TPS.2010.2042623

[20] Ramsey, N. F., *Molecular Beams*, Oxford Univ. Press, New York, 1990, p. 13.

[21] Kuharski, R. A., Mandell, M. J., Gardner, B. M., Katz, I., and Vaughan, D., "Ion Engine Neutralizer Erosion in Lab and Space," AIAA Paper 2005-3880, July 2005.

[22] Clausing, P., "The Formation of Beams in Molecular Streaming," *Zeitschrift für Physik*, Vol. 66, Nos. 7–8, 1930, pp 471–476. doi:10.1007/BF01402029

[23] Soulas, G. C., "Neutral Flux and Density Surrounding a Cylindrical Aperture in the Free Molecular Flow Regime," NASA TM (to be published).

[24] Dayton, B. B., "Gas Flow Patterns at Entrance and Exit of Cylindrical Tubes," *National Symposium on Vacuum Technology Transactions*, Pergamon, New York, 1956, pp. 5–11.

[25] Williams, G. J., Smith, T. B., Domonkos, M. T., Shand, K. J., Gallimore, A. D., and Drake, R. P., "Laser Induced Fluorescence Characterization of Ions Emitted from Hollow Cathode," AIAA Paper 1999-2862, June 1999.

[26] Mikellides, I. G., Katz, I., Goebel, D. M., and Polk, J. E., "Hollow Cathode Theory and Experiment II: A Two-Dimensional Theoretical Model of the Emitter Region," *Journal of Applied Physics*, Vol. 98, No. 11, 2005, Paper 113303. doi:10.1063/1.2135409

[27] Mikellides, I. G., Katz, I., Goebel, D. M., and Polk, J. E., "Theoretical Model of a Hollow Cathode Insert Plasma," AIAA Paper 2004-3817, July 2004.
[28] Grubisic, A. N., and Gabriel, S. B., "Hollow Cathode Thrust Mechanisms," AIAA Paper 2009-4823, Aug. 2009.
[29] Jameson, K. K., Goebel, D. M., and Watkins, R. M., "Hollow Cathode and Keeper-Region Plasma Measurements," AIAA Paper 2005-3667, July 2005.
[30] Polk, J. E., Goebel, D. M., Snyder, J. S., Schneider, A. C., Johnson, L. K., and Sengupta, A., "Performance and Wear Test Results for a 20 kW-Class Ion Engine with Carbon–Carbon Grids," AIAA Paper 2005-4393, July 2005.
[31] Van Noord, J. L., "NEXT Ion Thruster Thermal Model," AIAA Paper 2007-5218, July 2005.
[32] Herman, D. A., "The Use of Electrostatic Probes to Characterize the Discharge Plasma Structure and Identify Discharge Cathode Erosion Mechanisms in Ring-Cusp Ion Thrusters," Ph.D. Dissertation, Univ. of Michigan, Ann Arbor, MI, 2005.
[33] Herman, D. A., and Gallimore, A. D., "Discharge Chamber Plasma Structure of a 30-cm NSTAR-Type Ion Engine," AIAA Paper 2004-3794, July 2004.
[34] Aston, G., and Wilbur, P. J., "Ion Extraction from a Plasma," *Journal of Applied Physics*, Vol. 52, No. 4, April 1981, pp. 2614–2626. doi:10.1063/1.329071
[35] Farnell, C. C., Williams, J. D., and Wilbur, P. J., "Characteristics of Energetic Ions Emitted from Hollow Cathodes," International Electric Propulsion Conference, Electric Rocket Propulsion Soc. Paper 03-072, Fairview Park, OH, March 2003.
[36] Jameson, K. K., Goebel, D. M., and Watkins, R. M., "Hollow Cathode and Keeper-Region Plasma Measurements," AIAA Paper 2005-3667, July 2005.
[37] Foster, J. E., and Patterson, M. J., "Characterization of Downstream Ion Energy Distributions from a High Current Hollow Cathode in a Ring Cusp Discharge Chamber," AIAA Paper 2003-4865, July 2003.
[38] Bevington, P. R., *Data Reduction and Error Analysis for the Physical Sciences*, McGraw–Hill, New York, 1969, Chap. 4.

L. King
Associate Editor